Injection-Induced Flows in Porous-Walled Ducts

Robert A. Beddini*
University of Illinois at Urbana-Champaign, Urbana, Illinois

A theoretical analysis of the flow in porous-walled tubes and channels with appreciable injection through the duct wall is presented. Emphasis is placed on flows induced solely from injection by closure of a duct end. Effects of compressibility, nonideal boundary conditions, and turbulent transition on flow development are considered. The analysis employs a full Reynolds stress model of turbulence, with an implicit finite difference procedure used to solve the resulting parabolic equation system. Theoretical results, together with existing experimental data, indicate that the flows in porous tubes at large injection Reynolds numbers can undergo at least three regimes of flow development, proceeding from the closed head end. In the first regime, the velocity field develops in accordance with laminar similarity theory. In the second, high levels of turbulence are developed while the mean velocity field continues to correspond with laminar theory. The third regime commences with transition of the mean axial distribution, a process occurring at extremely large axial-flow Reynolds numbers.

Nomenclature

c_p = specific heat at constant pressure
h = specific sensible enthalpy
k = thermal conductivity
k_s = equivalent sand roughness height
p = static pressure
q = turbulence intensity, $= \overline{(u'^i u_i')}^{1/2}$
q_m = maximum value of q
R = inner radius of a cylindrical duct
R_u = universal gas constant
Re_b = bulk-flow Reynolds number (based on hydraulic diameter)
Re_c = axial-flow Reynolds number, $= \bar{\rho}_c \bar{u}_c \delta / \mu_c$
Re_s = injection Reynolds number, $= \bar{\rho}_s \bar{v}_s \delta / \bar{\mu}_s$
Re_t = turbulence Reynolds number, $= \bar{\rho} q \Lambda / \mu$
Ru = universal gas constant
t = time
T = static temperature
u_j = velocity vector (u,v,w)
$\bar{W}_{av}$ = average molecular weight of gas
x_j = coordinate vector (x,r,z)
x_0 = axial distance at which computational initial conditions are specified
y = distance from surface; $\delta - r$ (planar flow) or $R - r$ (axisymmetric flow)
β = momentum-flux coefficient, $= \int \overline{\rho u^2} dA / \rho_b u_b^2 A$
δ = half-height of planar duct or radius, R, of axisymmetric duct
Λ = turbulence macro-length scale
μ = viscosity
ρ = density
σ = k/c_p
σ_v = $[\overline{v'v'}/\overline{v^2}|_s]^{1/2}$

Superscripts

$(\bar{\ })$ = average of variable
$(\ )'$ = turbulent fluctuating value of variable

Subscripts

b = bulk (cross-sectionally averaged condition)
c = centerline
h = condition of port head end
s = condition at surface
$(\ ),$ = differentiation

Introduction

THE analysis of flow in planar (two-dimensional) and axisymmetric ducts with appreciable fluid injection through a permeable duct wall has been the subject of several prior investigations. In the present study, emphasis is placed on flows induced solely from injection, i.e., by closure of a duct end (Fig. 1). Experimental realizations of the basic flow are most often accomplished by using parallel porous plates or a cylindrical porous tube to provide the planar or axisymmetric duct geometries. Direct applications of these configurations have been noted in the literature, such as flow filtration and the diffusive separation of gaseous isotopes. In addition, the basic flow is approximately realized when a condensed-phase material on an impermeable duct surface undergoes gasification. The latter case is particularly relevant to ablative cooling devices, the evaporation sections of heat pipes, and the combustion-induced flowfield in solid-propellant rocket engines.

Unless otherwise noted, the analyses referred to in this section assume that the flow is steady in the mean, incompressible, has no net body force acting on it, and that material properties are constant. The term "transpiration" is used to collectively refer to injection and suction, since both effects have been considered in some analytical investigations. A more detailed literature review is given in Ref. 1.

A principal similarity parameter entering into the normalized equations of motion is the injection Reynolds number, $Re_s = \rho_s v_s \delta / \mu_s$, where the subscript s refers to conditions at the duct surface, v_s is the injection velocity, and δ is the radius of a cylindrical duct or the half-height of a planar channel. For the limiting case $Re_s \to \infty$, the laminar analyses of Taylor,[2] Yuan and Finkelstein,[3] Donaldson,[4] and Culick[5] yielded

$$\frac{u}{u_c} = \cos\left[\frac{\pi}{2}\left(\frac{r}{\delta}\right)^{v+1}\right] \tag{1}$$

where $u(x,r)$ is the axial velocity, $u_c(x)$ the axial velocity on the centerline (or centerplane), and $v = 0$ or 1 for planar or axisymmetric flows. Taylor compared Eq. (1) with his own

Received July 30, 1985; revision received March 18, 1986.

*Assistant Professor, Department of Aeronautical and Astronautical Engineering and Department of Mechanical and Industrial Engineering. Member AIAA.

experimental data and found the agreement to be "striking." Thus, a rare and simple solution to an inviscid system was found that also satisfied the no-slip boundary condition of the full Navier-Stokes equations.

Bankston and Smith[6] solved the laminar Navier-Stokes equations using a finite-difference method. Their results indicated that Eq. (1) became valid within a few radii of the closed (impermeable) fore end of the duct for values of Re_s of order 10^2 and larger. Varapaev and Yagodkin[7] investigated the viscous stability of flow in a channel at large injection Reynolds numbers. Relative to the stability of uninjected channel flow, the results with injection showed that 1) neutral stability occurred at lower axial-flow Reynolds numbers for values of injection Reynolds number less than 300, and 2) the axial-flow Reynolds number at neutral stability increased linearly for large values of injection Reynolds numbers.

Sviridenkov and Yagodkin[8] assumed the flow to be incompressible, and solved the fully elliptic, time-averaged, two-dimensional Navier-Stokes equations using a finite difference method. Turbulence closure was affected using either the "k-ϵ" model of Spalding[9] or the "k-ω" model of Launder and Spalding.[10] The objective of this study was to analytically assess the influence of injection Reynolds number on the "transition point"; approximately defined as the axial location within the duct at which small disturbances (or low turbulence levels) initially present within the flow become greatly amplified. The results indicated that the two turbulence models gave quantitatively and qualitatively different predictions of the transition point, with the Launder-Spalding model yielding fair agreement with the transition point data of Yagodkin.[11] While the Launder-Spalding turbulence model proved satisfactory in the pretransition region, it tended to overpredict turbulence levels (by approximately a factor of 3) in the fully turbulent post-transition region.

Experimental investigations performed at very large injection and axial-flow Reynolds numbers have surprisingly revealed that the flow is highly turbulent over most of the duct cross section, although the laminar theory velocity profile given by Eq. (1) persists in the mean. This was observed by Wageman and Guevara,[12] Yamada et al.,[13] and Dunlap et al.[14] These studies obtained values of Re_c of order 10^5 at relative duct lengths, x/δ, up to 36, where transition in the shape of the mean velocity profile would be expected based on classical pipe or channel flow results.

Beddini[15] analyzed planar compressible and reactive flows in porous channels employing a Reynolds stress turbulence closure model. For Re_s values approximating those of Yamada et al.,[13] transition was predicted to occur at relative channel lengths greater than those used in the experiments. It is emphasized that transition of the mean velocity profile has been observed in the lower Re_s investigations of Olson and Eckert[16] and Huesmann and Eckert.[17] These experiments covered the same Re_s and Re_c range of Yagodkin's results, who, however, did not observe transition of the mean flow.

The objective of the present study is to analyze the transitional characteristics of the flow in porous-walled ducts over a broad range of injection Reynolds numbers. The theoretical predictions may, therefore, serve to identify parameters influencing the transitional behavior, and may also guide future experimental investigations of this interesting type of flow.

Analysis

Governing Equations and Turbulence Closure

The fluid is assumed to be a compressible, perfect gas in the absence of body forces and governed by the Navier-Stokes equations. The ensemble- or time-averaging of the gas-phase equation system introduces the familiar problem of turbulence closure. Considering the nonequilibrium nature of turbulence development revealed in experimental studies

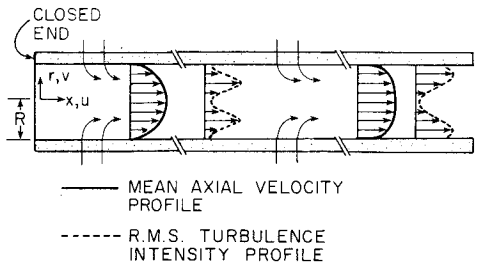

Fig. 1 Schematic representation of injection-induced porous-tube flows including transitional development.

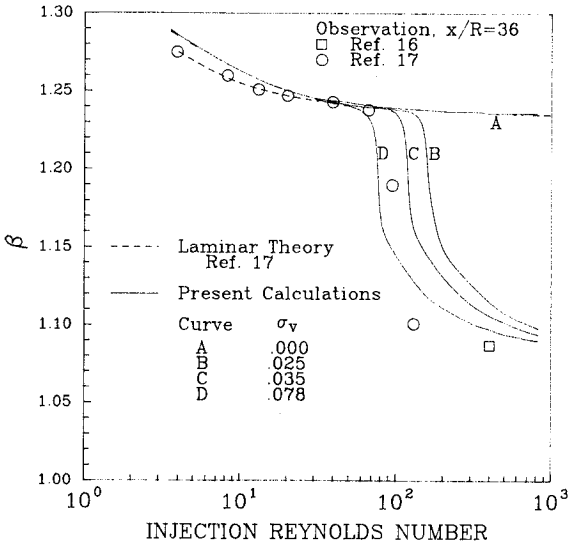

Fig. 2 Variation of momentum-flux coefficient with injection Reynolds number.

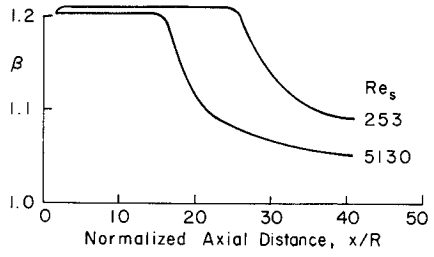

Fig. 3 Behavior of momentum-flux coefficient as a function of axial position.

of porous-tube flow and the deficiencies noted in prior analytical investigations using eddy diffusivity or turbulence kinetic energy closures, a more comprehensive turbulence closure approach appears desirable. Accordingly, the present investigation employs the second-order closure approach developed by Donaldson and colleagues.[18-20] This approach was implemented in Ref. 15 for planar reactive flows in porous channels, and is presently extended to axisymmetric flows.

Due to the tensor form of the turbulence models used to close the averaged equation system, no additional empirical modeling is required. Substitution of the metrics for an axisymmetric coordinate system is a straightforward but tedious process, aided at stages by symbolic manipulation software.[1] The thin-shear-layer (parabolization) assumptions are then implemented, and the mean radial pressure gradient is neglected because it may be shown to be of order $(\gamma-1)M_s^2 \ll 1$. (The resulting equation system is given in the Appendix. Values of the empirical turbulence modeling

parameters are given in Table A1, and are the same as those used in Ref. 15.)

Although differential equations for the turbulence macrolength scale, Λ, have been explored in prior studies, an algebraic relation is found to be more stable and well suited for this turbulence model for investigations of wall-bounded flows. The ramp-function equation for Λ is also given in the Appendix; $\Lambda(x,y)$ is constant with the value Λ_s near the wall, grows linearly with y in an intermediate region, and remains constant in the central region of the duct.

The parabolic differential equation system may be considered in the functional form

$$\bar{\rho}\bar{u}\frac{\partial f}{\partial x}+\bar{\rho}\bar{v}\frac{\partial f}{\partial r}=\frac{1}{r^{\nu}}\frac{\partial}{\partial r}\left(r^{\nu}\bar{\mu}_f\frac{\partial f}{\partial r}\right)+G_f(f) \qquad (2)$$

where

$$f=\{\bar{u},\bar{h},\ \overline{u'u'},\ \overline{v'v'},\ \overline{w'w'},\ \overline{u'v'},\ \overline{h'u'},\ \overline{h'v'},\ \overline{h'h'}\}^T$$

Here, u, v, and w are the axial, radial, and circumferential velocity components, respectively, ρ the density, and $h=c_pT$ the specific sensible static enthalpy. The molecular transport coefficient μ_f represents the dynamic viscosity μ or the thermal conductivity parameter, $\sigma=k/c_p$, as appropriate for each equation. However, not all of the molecular diffusion terms for each equation in the system may be cast in the form shown in Eq. (2). Those that do not conform are implicitly contained within the complex functions G_f, which also represent the sources, cross-coupling, and dissipation terms for the equations.

Boundary and Initial Conditions

Boundary conditions at the duct centerline (or centerplane) are the conventional symmetry conditions, which for the posed system are

$$\frac{\partial}{\partial r}[\bar{u},\bar{h},\ \overline{u'u'},\ \overline{v'v'},\ \overline{w'w'},\ \overline{h'h'},\ \overline{h'u'}]=0$$
$$=\overline{u'v'}=\overline{h'v'}=\bar{v}$$

At the duct surface, the static enthalpy corresponding to a given temperature is specified, and the mean injection velocity, $\bar{v}_s$, is prescribed. The no-slip condition implies that all tangential velocity components and their correlations are zero, i.e., $\bar{u}=\overline{u'u'}=\overline{u'v'}=\overline{w'w'}=0$. All enthalpy correlations are also null due to the prescribed uniform surface enthalpy.

It is the nonzero boundary condition on the unconstrained normal velocity component that provides a key theoretical point of the present investigation and that distiguishes it from prior porous-duct flow analyses and more general analyses of boundary layers with large injection rates. Experimental justification for nonzero $\overline{v'v'_s}$ may be found in Refs. 21 and 22. In the former study, air was injected through porous-plate samples without an external cross flow. Two sintered metal plates were fabricated using 1270- and 127-μm-diam particles, respectively. A hot-wire anemometer was then slowly traversed over the surface of each plate at a fixed height of 0.05 cm, while the injection velocity through the surface was increased (or decreased) after each complete traverse. The results of their anemometer traces for the 1270- and 127-μm plates showed that upon reaching a critical injection (surface) velocity: 1) positional fluctuations appear in the flow that are similar to turbulent fluctuations, however, they are stationary in time; 2) the length scale of these pseudoturbulent fluctuations is much larger than the diameter of the particles in the porous plates (a visual estimate suggests a factor of 10); and 3) the magnitude of the fluctuations increases with increasing average injection velocity.

Table A1 Numerical values of turbulence modeling parameters

$A=3.25$	$VRU=VRH=0.1$
$B=0.125$	$PMU2=PMH2=PMR2=1.0$
$CLAMB=0.17$	$PTHM=PTUM=0.15$
$DIN=0.65$	$PGH2=PGR2=0.8$
$AHH=5.85$	$PGU=PGU2=1.0$
$AHU=ARU=3.25$	$WWU1=WWR1=WWH1=-0.1$
$BHH=0.225$	$WWGU=-0.5$
$VUU=VUH=VHH=0.1$	$WWGR=WWGH=-1.0$

This pseudoturbulence phenomenon is discussed in more detail in Ref. 1. For the present, it is noted that such effects must be accounted for if an ensemble (or volume) averaging procedure is employed for the mean and fluctuating components of flow variables. In addition, it would be difficult to formally include this effect with a kinetic energy (k) closure, since the disturbance is in the v' component, with tangential components satisfying the no-slip condition. With the second-order closure model presently employed, the normalized surface pseudoturbulence parameter $\sigma_v=[\overline{v'v'}/\bar{v}^2|_s]^{1/2}$ is defined to investigate its effect on flow development.

Initial conditions for the calculations are prescribed profiles of the dependent variables at $x=x_0=2R$. The specific profiles employed are discussed in a subsequent section.

Numerical Solution Procedure

The numerical solution procedure for the differential equation system utilizes an implicit, Crank-Nicholson method. Symbolic manipulation software is again employed at this stage to yield the complex matrices on a term-by-term basis from the final equations directly coded in FORTRAN. Block decoupling of the nine dependent variables is used to accelerate the solution by using the tridiagonal algorithm. The largest subblock size solved is 3×3.

An unequally spaced, dynamically adaptive grid is employed in both the axial and radial directions. The radial mesh is varied inversely with the normalized curvature of selected dependent variables, allowing effective resolution of regions of rapid change of both mean flow and Reynolds stresses. To complete the solution procedure, $\bar{v}$ is found by quadrature of the continuity equation, and the axial pressure gradient is determined iteratively by satisfaction of global mass continuity over an axial step. Further details of the solution procedure may be found in Ref. 1.

The coordinate singularity at $r=0$ was numerically avoided by specifying the exact boundary condition at $r/R=0.01$. However, the $\overline{v'v'}$ and $\overline{w'w'}$ equations contain terms such as $(\overline{v'v'}-\overline{w'w'})/r^2$, which produced instabilities in the centerline region in initial calculations. Specifying $\overline{v'v'}=\overline{w'w'}$ within $r/R\leq0.15$ alleviated, but did not completely eliminate, these instabilities.

Results and Discussion

Transition Behavior at Lower Injection Reynolds Numbers

Experimental observations of mean-flow transition for injection-induced flows in porous tubes were made by Olson[16] and Huesmann-Eckert,[17] both experiments using essentially the same apparatus. The Huesmann-Eckert results were obtained for injection Reynolds numbers ranging from approximately 4 to 125, with the mean velocity profiles measured at a single axial location, $x/R=36$. For the higher injection Reynolds numbers, a transitional change in the shape of the mean velocity profiles was obtained.

Husemann and Eckert evaluated the integral momentum-flux coefficient, β, for each of the profiles as a function of injection Reynolds number and compared the results with laminar similarity theory, as shown in Fig. 2. The experimental data are seen to agree with laminar theory (broken line) up to a value of $Re_s\simeq60$. For larger values of Re_s, β drops below the laminar theory by about 15%. The value of β

observed by Huesmann and Eckert for $Re_s = 125$ approaches the value obtained by Olson at $Re_s = 400$, suggesting that transition of the mean flow is largely completed for $Re_s \gg 100$ in this particular experiment.

The calculations from the present theory, shown by the solid lines in Fig. 2, have been performed under the following nominal conditions. At the initial station of $x_0/R = 2$, the profiles of $\overline{u'u'}$, $\overline{v'v'}$, and $\overline{w'w'}$ are specified arbitrarily to be similar to the mean velocity profile [Eq. (1)] in shape. The relative rms intensity at the centerline is 0.017, and is partitioned among the velocity correlations as $2\overline{u'u'} = \overline{v'v'} = \overline{w'w'}$. For the calculations performed with finite $\overline{v'v'_s}$, the value of Λ_s is assumed to be 3×10^{-2} cm. Values of Λ within the range $2\text{-}10 \times 10^{-2}$ cm were found to be sufficiently large so as to prevent the immediate decay within the flow of disturbances introduced at the boundary and, hence, displayed little sensitivity to precise value. Other calculations were also performed to assess the effects of assumed initial Reynolds-stress profile shape and energy partitioning. Moving the radial location of maximum turbulence from $y/R = \frac{1}{2}$ to $\frac{1}{4}$ produced an initial convection of this maximum back into the region $y/R \simeq \frac{1}{2}$ within about 5 radii downstream of the initial station and, hence, yielded almost negligible downstream influence.

Considering the calculations shown in Fig. 2, it can be seen that the results obtained without surface-generated turbulence (curve A) are in good agreement with laminar theory. Although the calculated results in the figure are presented for $x/R = 36$, it is found that the continuations of the individual calculations (from which curve A is deduced) up to sonic conditions ($x/R \simeq 56$) also do not reveal transition. In addition, other calculations have been performed in which the initial relative rms turbulence intensities range up to 25%, while maintaining $\sigma_v = 0$. These results produced transtion beyond $x/R = 36$.

In contrast to the preceding results, the theoretical results obtained using finite values of surface-generated pseudo-turbulence (curves B, C, and D) show a pronounced effect on the value of Re_s associated with transition. This effect diminishes somewhat for larger values of surface intensity. The relative surface intensities, which yield the best quantitative agreement with the particular experimental data, are seen to lie in the range $0.035 \leq \sigma_v \leq 0.078$; a result that appears to be quite reasonable in view of the observations cited. The sensitivity of the theoretical results to the small levels of turbulence generated by the specific porous surface may therefore partly explain why other experimental investigators have not observed transition under similar mean-flow conditions.

Since Huesmann and Eckert obtained principal flow measurements as a function of Re_s at only one axial location, it is not possible to estimate the length or duration of the transition region from their data. However, the predicted variation of β as a function of x/R is shown in Fig. 3 for $Re_s = 253$ and 5130. The computational conditions correspond with those stated for curve C in Fig. 2. The values of Re_s are based on conditions near the head end of the tube although, due to the effects of compressibility and the assumed constancy of $\bar{v}_s$, injection Reynolds numbers are found to decrease by approximately 20% at $x/R = 36$. For either the moderately low value of $Re_s = 253$ or the high value of 5130, the predicted length of the mean-flow transition process is seen to be of the order of 5 radii. Beyond the immediate region of transition, each of the curves would, for incompressible flow, approach the impermeable tube value of $\beta \simeq 1.03$ (cf., Ref. 16) as Re_s/Re_c approaches zero at very large axial distances.

The mean axial velocity profiles measured by Huesmann and Eckert at $x/R = 36$ are shown in Fig. 4 for $Re_s = 64$, 94, and 126. Theoretical results are provided for $Re_s = 61$, 83, and 125 for approximate comparison with the data and with laminar theory [Eq. (1)]. The calculations have been performed under conditions corresponding with curve C in Fig. 2, viz., $\sigma_v = 0.035$. Qualitatively, the theoretical results are in good agreement with the data and demonstrate the behavior of mean flow during the transition process.

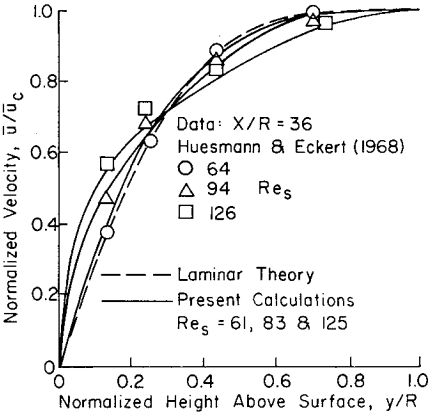

Fig. 4 Variation of mean axial velocity profiles with injection Reynolds number.

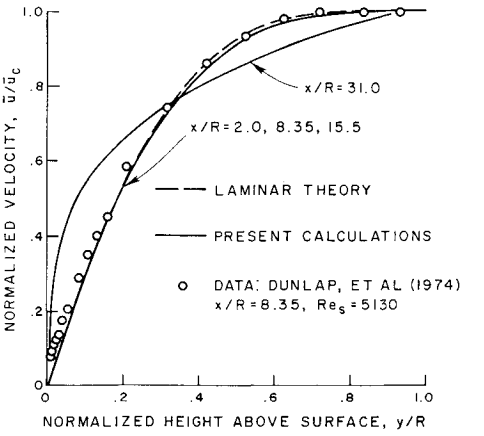

Fig. 5 Development of mean axial velocity profiles for injection-induced flow in a porous tube at $Re_{s1_{x=0}} = 5130$.

Predicted Transition Behavior at Large Re_s

In the experiment of Dunlap et al.,[14] five porous tube segments with individual flow-supply chambers were joined together to form a tube of 74.9 cm overall length and 4.84 cm radius. Although the presence of intersegment impermeable gaps of 0.25 and 0.84 cm in the porous surface may have affected some aspects of turbulence development, the use of individual flow-supply chambers permitted improved regulation of the overall constancy of injection rate along the tube surface. The principal flow measurements were obtained with a single-wire thermoanemometer at $x/R = 8.35$. Mean velocity profiles at this axial location were obtained for approximate injection Reynolds numbers ranging from 640 to 5130. Due to the relatively large injection Reynolds numbers, good agreement with Eq. (1) was obtained at $x/R = 8.35$ for all Re_s.

A comparison of theoretical results with the mean axial velocity profile data of Dunlap et al. is shown in Fig. 5 for $Re_s = 5130$. The initial and boundary conditions are chosen consistently with those described for the calculations shown in Fig. 3 and for curve C in Fig. 2, viz., $x_0 = 2R$ and $\sigma_v = 0.035$. The present calculations are seen to be in good agreement with the experimental data at $x/R = 8.35$ and also maintain agreement with laminar theory to the end of the experimental porous tube at $x/R = 15.5$. However, shortly beyond this axial location, the extended calculations begin to

show a transition to a turbulent velocity profile. The relative change in the shape of the velocity profile is reflected by the momentum-flux coefficient, β, as shown in Fig. 3. The normalized velocity profiles continue to "fill out" such that by $x/R = 31.0$ (Fig. 5) a profile approximated by $u/u_c = (y/R)^{0.25}$ is predicted.

The calculated rms turbulence intensity profiles are shown in Fig. 6 together with the experimental data at $x/R = 8.35$. The approximate distribution and overall magnitude of the data are predicted reasonably well by the theory. This may be considered fortuitous in view of the fact that the (experimentally unknown) initial conditions and the level of surface-generated pseudoturbulence for these calculations are prescribed in a manner consistent with the Huesmann-Eckert comparison, where the injection Reynolds numbers are a factor of 50 lower. Although not shown in Fig. 6, the results of calculations performed using a relative surface intensity of 7.8% produced a maximum turbulence intensity of approximately 1.7 m/s at $x/R = 8.35$, almost twice the level of the data. This again exemplifies the theoretical (and, by hypothesis, experimental) sensitivity to the level of disturbance induced by the surface.

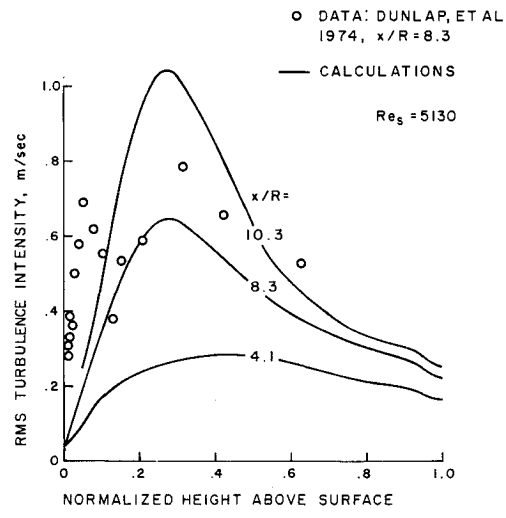

Fig. 6 Development of turbulence intensity for injection-induced flow in a porous tube.

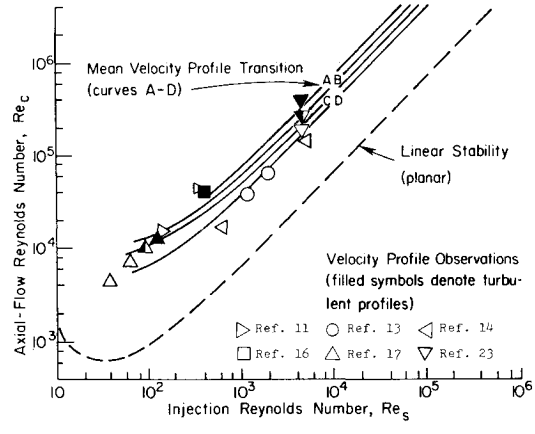

Fig. 7 Variation of axial-flow Reynolds numbers for stability and mean velocity transition with injection Reynolds number. Broken line: planar linear stability theory.[7] Solid lines: calculations for mean velocity profile transition. Curves: A—tube, high initial turbulence, no surface turbulence; B—tube, low initial turbulence, $\sigma_v = 0.35$; C—tube, low initial turbulence, $\sigma_v = 0.78$; D—channel, low initial turbulence, $\sigma_v = 0.78$.

Relation Between the Turbulent and Mean-Flow Transition Processes

Based upon their experimental results, Huesmann and Eckert hypothesized that the approximate coordinates $Re_s = 70$ and $Re_b = 10^4$ ($Re_c = 7.9 \times 10^4$) represented one point on an assumed quasiuniversal locus of mean-flow transition for porous tubes with injection. Another point on the hypothesized locus was represented by the limiting condition for an impermeable tube; i.e., $Re_s = 0$ and $Re_b = 2300$. However, it is well known that even this latter condition can be substantially altered by orders of magnitude above the nominal value of $Re_b = 2300$, due to the level of inlet or boundary disturbances experimentally introduced. Although a universal transition locus is not anticipated, it is nevertheless desirable to further investigate the functional dependence of mean-flow transition on injection Reynolds number under established theoretical conditions It is also of interest to investigate the relation between the initial laminar-to-turbulent transition of the flow and the subsequent transition of the mean velocity profile.

Figure 7 shows the behavior of the locus of neutral stability (assumed here to *qualitatively* represent destabilization and transition to flow turbulence) as determined by Varapaev and Yagodkin using linear, planar, viscous, nonparallel stability theory. Above this broken line are solid lines (curves A-D) which represent the loci of transition of the mean velocity profile, as determined from the present analysis under various conditions.

Considering the linear stability results of Varapaev and Yagodkin first, it is noted that for $Re_s = 0$ the neutral stability limit for planar Poiseuille flow ($Re_c \simeq 6000$) is obtained. For low values of injection Reynolds numbers ($Re_s < 37$), a reduction in the neutral stability value of Re_c is observed, indicating that lower injection rates destabilize the flow. For higher values of Re_s, the effects of favorable pressure gradients become more important and tend to appreciably increase the stability of the flow. A key result of the Varapaev and Yagodkin analysis is the linearity of the neutral stability value of Re_c as a function of Re_s for Re_s greater than about 300.

The calculated results for transition of the mean velocity profile (curves A-D) are based on observation of the precipitous drop in β (Figs. 2 and 3) to establish approximate coordinates of transition. It is seen that curves A-D are all linear at the higher values of Re_s, implying that the relative axial distance between destabilization of the flow (turbulent transition) and mean velocity profile transition is constant. The value of this constant depends on the initial and boundary conditions. For curve A, a very large level (25%) of initial turbulence at $x_0 = 2R$ produced the results shown. With lower levels of turbulence specified at this initial station and no surface-generated turbulence, the values of Re_c for transition increased substantially, eventually meeting the choking condition at $x/R \simeq 56$. The results denoted by curves B and C have been obtained with a relatively low level of initial turbulence and moderate levels of surface turbulence. (These conditions correspond with those discussed previously for curves C and D in Fig. 2.) As anticipated from Fig. 2, curves B and C show successively lower values of Re_c at transition. For curve B, the limiting value of x/R at transition is approximately 16.5 for large Re_s. By comparing curves C and D at large Re_s, it is seen that there is little difference (22%) between the predicted transition values of Re_c for a tube or channel under similar flow conditions.

The Huesmann-Eckert results, obtained at a constant value of $x/R = 36$ and varying Re_s, exhibit transition of the mean velocity profile upon crossing curve B. (The extent of quantitative agreement shown in the figure is due to the assumption of a specific level of surface-generated pseudoturbulence.) Noting that the behavior of curves B-D for $50 < Re_s < 300$ is similar to the trend exhibited by linear stability theory in that the functional dependence of Re_c (at

transition) on Re_s is less than linear, it is theoretically found that this is the only injection Reynolds number regime in which transition can be induced for constant x/R by variation of Re_s. This implies that the experimental apparatus of Dunlap et al., for example, would have to be modified by increasing the length of the tube or by increasing the effective disturbance level of the porous surface in order to yield transitional behavior of the mean flow at large Re_s.

Based upon the preceding predictions (informally reported in Ref. 1), Brown et al.[23] recently reported preliminary data from a porous tube similar to, but longer than, that employed by Dunlap et al. Profiles of mean flow and turbulence were measured at several axial stations (increasing Re_c at constant Re_s). As shown in Fig. 7, the new experimental data qualitatively, and, to a good degree, quantitatively confirm the theoretical results presented.

Summary and Conclusions

For large injection Reynolds numbers, the flow development in porous ducts is characterized by three distinct regimes. Within a relative axial distance of $x/R<5$, as measured from the closed (head) end, the axial velocity profile attains the form predicted by laminar similarity theory. For relative axial distances less than 10, the flow can undergo a turbulent transition with turbulence intensities greater than 10% of the axial velocity component observed. Within this second regime, the mean axial velocity profile continues to correspond with laminar similarity theory, while the turbulence intensity profile undergoes further development. The pronounced maximum in the turbulence intensity profile lies midway between the centerline and the inner surface of the tube at values of $x/R<10$. The height above the surface at which this maximum occurs decreases with increasing axial distance. A third flow regime has been predicted and experimentally observed, and is initiated by transition of the mean axial velocity profile.

The sensitivity of turbulence development in the second regime and the attendant mean-flow transition process have been assessed for two types of disturbance. The first type originates within the head-end region ($x/R\leq 1$), as caused, for example, by the vortex/turbulence shedding off the impermeable head-end surface. This type is simulated by specifying finite relative turbulence intensity distributions as computational initial conditions. The second type of disturbance is caused by high fluid injection rates through a porous medium—the "pseudoturbulence" phenomenon experimentally observed as the flow issues from the surface. The results of the sensitivity studies may be summarized as follows.

1) For either type of disturbance and for any of the disturbance levels investigated, the present results for the loci of axial-flow Reynolds number at mean-flow transition ($Re_{c,\mathrm{tr}}$) as a function of injection Reynolds number (Re_s) follow the trend predicted by planar linear stability theory for the initial destabilization (turbulent transition) of the flow. In particular, for large values of Re_s (>300) the present results indicate the linear relation $Re_{c,\mathrm{tr}}\simeq Re_s$ with the constant of proportionality generally dependent on the magnitude and type of disturbance.

2) The growth rates of the maximum value of turbulence and the downstream location of mean-flow transition are quite sensitive to the relative turbulence level specified at the initial station when this level is small (less than 5% of the mean speed). In such cases, the tube lengths required for mean-flow transition can be relatively large ($x/R>50$), and the present compressible flow calculations indicate that the flow can choke before mean-flow transition is attained.

3) The location of transition becomes nearly insensitive to relative initial turbulence levels when such levels are large (greater than approximately 15%). The "excess" turbulence is found to decay in the upstream portion of regime 2.

4) Disturbances introduced at the porous-tube surface are predicted to be much more effective in inducing transition than are disturbances introduced within the upstream region of the flow.

Appendix

The final equations for mean-velocity, enthalpy, Reynolds stresses, Reynolds heat-flux correlations, and the state and macro-length scale equations are given below. The numerical values of the turbulence modeling parameters are given in Table A1.

$$(\bar\rho\bar u)_{,x}+r^{-\nu}[r^{\nu}(\bar\rho\bar v+\overline{\rho' v'})]_{,r}=0 \tag{A1}$$

$$\bar\rho\bar u\bar u_{,x}+(\bar\rho\bar v+\overline{\rho' v'})\bar u_{,r}+r^{-\nu}(r^{\nu}\bar\rho\overline{u' v'})_{,r}=r^{-\nu}(r^{\nu}\bar\mu\bar u_{,r})_{,r}-\bar p_{,x} \tag{A2}$$

$$\bar\rho\bar u\bar h_{,x}+(\bar\rho\bar v+\overline{\rho' v'})\bar h_{,r}+r^{-\nu}(r^{\nu}\bar\rho\overline{h' v'})_{,r}=r^{-\nu}(r^{\nu}\bar\sigma\bar h_{,r})_{,r}+\bar u\bar p_{,x}+\bar\mu[(\bar u_{,r})^2+(A+B\cdot Re_t)(q^2/\Lambda^2)] \tag{A3}$$

$$\begin{aligned}&\bar\rho(\bar u\overline{u' u'_{,x}}+\bar v\overline{u' u'_{,r}})+2\overline{\rho' u'}(\bar u\bar u_{,x}+\bar v\bar u_{,r})-r^{-\nu}(r^{\nu}\overline{\rho' v'})_{,r}\overline{u' u'}-2\cdot VRU\cdot q\Lambda\overline{\rho' u'_{,r}}\bar u_{,r}+2\bar\rho(\overline{u' u'}\bar u_{,x}+\overline{u' v'}\bar u_{,r})\\&-r^{-\nu}(VUU\bar\rho q\Lambda r^{\nu}\overline{u' u'_{,r}})_{,r}=2\cdot(PGU2\cdot WWGU+B)(\bar\rho q/\Lambda)[\overline{u' u'}-(q^2/3)]+r^{-\nu}(\bar\mu r^{\nu}\overline{u' u'_{,r}})_{,r}\\&-2\bar\mu(A+B\cdot Re_t)(\overline{u' u'}/\Lambda^2)]+\bar\mu_{,r}[\overline{u' u'_{,r}}+(\overline{v' v'}/2)+\nu r^{-1}(\overline{v' v'}-\overline{w' w'})]+2\bar\mu_{,h}\overline{h' u'_{,r}}\bar u_{,r}+2\bar\mu_{,h}\overline{h' u'}r^{-\nu}(r^{\nu}\bar u_{,r})_{,r}\end{aligned} \tag{A4}$$

$$\begin{aligned}&\bar\rho(\bar u\overline{v' v'_{,x}}+\bar v\overline{v' v'_{,r}})-r^{-\nu}(r^{\nu}\overline{\rho' v'})_{,r}\overline{v' v'}+2\bar\rho\bar v_{,r}\overline{v' v'}-r^{\nu}(VUU\cdot\bar\rho q\Lambda r^{\nu}\overline{v' v'_{,r}})_{,r}-2(VUU\cdot\bar\rho q\Lambda\overline{v' v'_{,r}})_{,r}\\&-2\cdot VUU\cdot\bar\rho q\Lambda\nu r^{-1}(\overline{v' v'}-\overline{w' w'})_{,r}+4\cdot VUU\cdot\bar\rho q\Lambda\nu r^{-2}(\overline{v' v'}-\overline{w' w'})=-2\cdot PMU2\cdot WWU1\cdot\{(\bar\rho q\Lambda\overline{v' v'_{,r}})\\&-\nu[\bar\rho q\Lambda r^{-1}(v' v'-w' w')]\}_{,r}+2(PGU2\cdot WWGU+B)(\bar\rho q/\Lambda)[\overline{v' v'}-(q^2/3)]+r^{-\nu}(\bar\mu r^{\nu}\overline{v' v'_{,r}})_{,r}\\&-2\nu r^{-2}\bar\mu(\overline{v' v'}-\overline{w' w'})-2\bar\mu(A+B\cdot Re_t)(\overline{v' v'}/\Lambda^2)+\bar\mu_{,r}\overline{v' v'_{,r}}\end{aligned} \tag{A5}$$

$$\begin{aligned}&\bar\rho(\bar u\overline{w' w'_{,x}}+\bar v\overline{w' w'_{,r}})-r^{-\nu}(r^{\nu}\overline{\rho' v'})_{,r}\overline{w' w'}+2\nu r^{-1}\bar\rho\bar v\overline{w' w'}-r^{-\nu}(VUU\cdot\bar\rho q\Lambda r^{\nu}\overline{w' w'_{,r}})_{,r}+2\nu[VUU\cdot\bar\rho q\Lambda r^{-1}(\overline{w' w'}-v' v')]_{,r}\\&-2\nu\cdot VUU\cdot\bar\rho q\Lambda r^{-1}\overline{w' w'_{,r}}+4\nu\cdot VUU\cdot\bar\rho q\Lambda r^{-2}(\overline{w' w'}-\overline{v' v'})=-2\nu\cdot PMU2\cdot WWU1\cdot r^{-1}\bar\rho q\Lambda[\overline{v' v'_{,r}}-r^{-1}(\overline{w' w'}-\overline{v' v'})]\\&+2(PGU2\cdot WWGU+B)(\bar\rho q/\Lambda)[(\overline{w' w'}-(q^2/3)]+r^{-\nu}(\bar\mu r^{\nu}\overline{w' w'_{,r}})_{,r}-2r^{-2}\bar\mu(\overline{w' w'}-\overline{v' v'})\\&-2\bar\mu(A+B\cdot Re_t)\overline{w' w'}+\bar\mu_{,r}\overline{w' w'_{,r}}-3/2\ \nu r^{-1}\bar\mu(\overline{w' w'}-\overline{v' v'})+\tfrac{1}{2}\bar\mu_{,r}\overline{v' v'_{,r}}\end{aligned} \tag{A6}$$

$$\bar{\rho}(\bar{u}\overline{u'v'_{,x}}+\bar{v}\overline{u'v'_{,r}})+\overline{\rho'v'}(\bar{u}\bar{u}_{,x}+\bar{v}\bar{u}_{,r})-2\cdot VRU\cdot\overline{\rho'v'_{,r}}q\Lambda\bar{u}_{,r}-r^{-\nu}(r^{\nu}\overline{\rho'v'})_{,r}\overline{u'v'}+\bar{\rho}(\overline{u'v'}\bar{u}_{,x}+\overline{v'v'}\bar{u}_{,r})+\bar{\rho}\bar{v}_{,r}\overline{u'v'}$$
$$-2r^{-\nu}(VUU\cdot\bar{\rho}q\Lambda\overline{u'v'_{,r}})_{,r}+2\nu r^{-2}\cdot VUU\cdot\bar{\rho}q\Lambda\overline{u'v'}=-[PMU2\cdot WWU1\bar{\rho}q\Lambda r^{-\nu}(r^{\nu}\overline{u'v'})_{,r}]_{,r}$$
$$+2\cdot PGU2\cdot WWGU\cdot(\bar{\rho}q/\Lambda)\overline{u'v'}+[\bar{\mu}r^{-\nu}(r^{\nu}\overline{u'v'})_{,r}]_{,r}-2\bar{\mu}A(\overline{u'v'}/\Lambda^2)+3/2\,\bar{\mu}_{,r}\overline{u'v'}-\tfrac{1}{4}\bar{\mu}_{,r}r^{-\nu}(r^{\nu}\overline{u'v'})_{,r}$$
$$+\bar{\mu}_{,h}\overline{h'v'_{,r}}\bar{u}_{,r}+r^{-\nu}(\bar{\mu}_{,h}\overline{h'v'}r^{\nu}\bar{u}_{,r})_{,r} \tag{A7}$$

$$\bar{\rho}(\bar{u}\overline{h'u'_{,x}}+\bar{v}\overline{h'v'_{,r}})+\overline{\rho'u'}(\bar{u}\bar{h}_{,x}+\bar{v}\bar{h}_{,r})+\overline{\rho'h'}(\bar{u}\bar{u}_{,x}+\bar{v}\bar{u}_{,r})-r^{-\nu}(VUH\cdot\bar{\rho}q\Lambda r^{\nu}\overline{h'u'_{,r}})_{,r}-VRH\cdot q\Lambda\overline{\rho'h'_{,r}}\bar{u}_{,r}-VRU\cdot q\Lambda\overline{\rho'u'_{,r}}\bar{h}_{,r}$$
$$-r^{-\nu}(r^{\nu}\overline{\rho'v'})_{,r}\overline{h'u'}+\bar{\rho}(\overline{u'u'}\bar{h}_{,x}+\overline{u'v'}\bar{h}_{,r})+\bar{\rho}(\overline{h'u'}\bar{u}_{,x}+\overline{h'v'}\bar{u}_{,r})=\overline{u'u'}\bar{p}_{,x}+PGH2\cdot WWGH\cdot(\bar{\rho}q/\Lambda)\overline{h'u'}$$
$$-\bar{\mu}(AHU+BHU\cdot Re_t)(\overline{h'u'}/\Lambda^2)-\tfrac{1}{2}\,\bar{\mu}_{,h}\overline{h'u'_{,r}}\bar{u}_{,r}+r^{-\nu}(\bar{\mu}_{,h}\overline{h'h'}r^{\nu}\bar{u}_{,r})_{,r}+\bar{\mu}(\overline{u'u'_{,r}}+\tfrac{1}{2}\overline{v'v'_{,r}})\bar{u}_{,r}$$
$$+\tfrac{1}{2}\nu r^{-1}\bar{\mu}(\overline{v'v'}-\overline{w'w'})\bar{u}_{,r}+\bar{\mu}_{,h}\overline{h'u'}(\bar{u}_{,r})^2+r^{-\nu}(\bar{\sigma}r^{\nu}\overline{h'u'_{,r}})_{,r}-\bar{\sigma}(AHU+BHU\cdot Re_t)(\overline{h'u'}/\Lambda^2)$$
$$+\bar{\sigma}_{,r}\bar{h}_{,r}+r^{-\nu}(\bar{\sigma}_{,h}\overline{h'u'}r^{\nu}\bar{h}_{,r})_{,r}+\bar{\sigma}_{,h}\overline{h'u'_{,r}}\bar{h}_{,r} \tag{A8}$$

$$\bar{\rho}(\bar{u}\overline{h'v'_{,x}}+\bar{v}\overline{h'v'_{,r}})+\overline{\rho'v'}(\bar{u}\bar{h}_{,x}+\bar{v}\bar{h}_{,r})-2r^{-\nu}(VUH\cdot\bar{\rho}q\Lambda r^{\nu}\overline{h'v'_{,r}})_{,r}+2\nu r^{-2}\cdot VUH\cdot\bar{\rho}q\Lambda\overline{h'v'}-2\cdot VRU\cdot q\Lambda\overline{\rho'v'_{,r}}\bar{h}_{,r}$$
$$-r^{-\nu}(r^{\nu}\overline{\rho'v'})_{,r}\overline{h'v'}+\bar{\rho}(\overline{u'v'}\bar{h}_{,x}+\overline{v'v'}\bar{h}_{,r})+\bar{\rho}\bar{v}_{,r}\overline{h'v'}=\overline{u'v'}\bar{p}_{,x}-[PMH2\cdot WWH1\cdot\bar{\rho}q\Lambda r^{-\nu}(r^{\nu}\overline{h'v'})_{,r}]_{,r}$$
$$-\bar{\mu}(AHU+BHU\cdot Re_t)(\overline{h'v'}/\Lambda^2)+\bar{\mu}\overline{u'v'_{,r}}\bar{u}_{,r}+\tfrac{1}{2}\bar{\mu}r^{-\nu}(r^{\nu}\overline{u'v'}\bar{u})_{,r}+\bar{\mu}_{,h}\overline{h'v'}(\bar{u}_{,r})^2+[\bar{\sigma}r^{-\nu}(r^{\nu}\overline{h'v'})_{,r}]_{,r}$$
$$-\bar{\sigma}(AHU+BHU\cdot Re_t)(\overline{h'v'}/\Lambda^2)+\bar{\sigma}_{,r}\overline{h'v'_{,r}}+\bar{\sigma}_{,h}\overline{h'v'}r^{-\nu}(r^{\nu}\bar{h}_{,r})_{,r}+\bar{\sigma}_{,h}\overline{h'v'_{,r}}\bar{h}_{,r} \tag{A9}$$

$$\bar{\rho}(\bar{u}\overline{h'h'_{,x}}+\bar{v}\overline{h'h'_{,r}})+2\overline{\rho'h'}(\bar{u}\bar{h}_{,x}+\bar{v}\bar{h}_{,r})-r^{-\nu}(VHH\bar{\rho}q\Lambda r^{\nu}\overline{h'h'_{,r}})_{,r}-r^{-\nu}(r^{\nu}\overline{\rho'v'})_{,r}\overline{h'h'}+2\bar{\rho}(\overline{h'u'}\bar{h}_{,x}+\overline{h'v'}\bar{h}_{,r})$$
$$-2\cdot VRH\cdot q\Lambda\overline{\rho'h'_{,r}}\bar{h}_{,r}=2\overline{h'u'}\bar{p}_{,x}+2\bar{\mu}_{,h}\overline{h'h'}(\bar{u}_{,r})^2+r^{-\nu}(\bar{\sigma}r\overline{h'h'_{,r}})_{,r}-2\bar{\sigma}(AHH+BHH\cdot Re_t)(\overline{h'h'}/\Lambda^2)$$
$$+2r^{-\nu}\bar{\sigma}_{,h}(r^{\nu}\overline{h'h'_{,r}})_{,r}+\bar{\sigma}_{,h}\overline{h'h'_{,r}}\bar{h}_{,r} \tag{A10}$$

$$\bar{p}=(R_u\bar{\rho}\bar{h}/c_pW_{av})[1-(\overline{h'h'}/\bar{h}^2)]^{-1} \tag{A11}$$

$$\Lambda(x,y)=\min[\Lambda_s+DIN\cdot y, CLAMB\cdot\delta] \tag{A12}$$

Acknowledgments

This research was sponsored by the Air Force Office of Scientific Research (AFSC). Thesis research was performed at Rutgers University under the advice of Professor Richard Peskin and conducted, in part, under a cooperative program while the author was employed by Aeronautical Research Associates of Princeton, Inc. The author greatly appreciates the personal communication of turbulence intensity data by Dr. R. Dunlap.

References

[1]Beddini, R. A., "Analysis of Injection-Induced Flows in Porous-Walled Ducts with Application to the Aerothermochemistry of Solid-Propellant Motors," Ph.D. Thesis, Rutgers University, New Brunswick, NJ, Oct. 1981.

[2]Taylor, G. I., "Fluid Flow in Regions Bounded by Porous Surfaces," *Proceedings of the Royal Society of London*, Series 234A, Vol. 1199, 1956, pp. 456-475.

[3]Yuan, S. W. and Finkelstein, A. B., "Laminar Pipe Flow with Injection and Suction Through a Porous Wall," *Transactions of the ASME*, Vol. 28, 1956, pp. 719-724.

[4]Donaldson, C. duP., "Solutions of the Navier-Stokes Equations for Two- and Three-Dimensional Vortices," Ph.D. Thesis, Princeton University, Princeton, NJ, 1956.

[5]Culick, F. E. C., "Rotational Axisymmetric Mean Flow and Damping of Acoustic Waves in Solid Propellant Rocket Motors," *AIAA Journal*, Vol. 4, Aug. 1966, pp. 1462-1464.

[6]Bankston, C. A. and Smith, H. J., "Vapor Flow in Cylindrical Heat Pipes," *Journal of Heat Transfer*, Vol. 95, Aug. 1973, pp. 371-376.

[7]Varapaev, V. N. and Yagodkin, V. I., "Flow Stability in a Channel with Porous Walls," *Izv. A. N. SSSR, Mechanika Zhidkosti i Gaza*, Vol. 4, No. 5, 1969, pp. 91-95.

[8]Sviridenkov, A. A. and Yagodkin, V. I., "Flows in the Initial Sections of Channels with Permeable Walls," *Izv. A. N. SSSR, Mechanika Zhidkosti i Gaza*, Vol. 11, No. 5, 1976, pp. 43-48.

[9]Spalding, D. B., "A Two-Equation Model of Turbulence," *VDI-Forschungsheft*, Vol. 549, 1972, p. 76.

[10]Launder, B. E. and Spalding, D. E., "The Numerical Computation of Turbulent Flows," *Computational Methods in Applied and Mechanical Engineering*, Vol. 3, 1974, pp. 122-129.

[11]Yagodkin, V. I., "Use of Channels with Porous Walls for Studying Flows Which Occur During Combustion of Solid Propellants," translated from *Proceedings of the 18th Astronautics Congress*, Pergamon Press and Panstwowe, Wydawnichtwo Naukowe, Poland, Vol. 3, 1967, pp. 69-79.

[12]Wageman, W. E. and Guevara, F. A., "Fluid Flow Through a Porous Channel," *The Physics of Fluids*, Vol. 3, No. 6, 1960, pp. 878-881.

[13]Yamada, K., Goto, M., and Ishikawa, N., "Simulative Study on the Erosive Burning of Solid Rocket Motors," *AIAA Journal*, Vol. 14, Sept. 1976, pp. 1170-1176.

[14]Dunlap, R., Willoughby, P. G., and Hermsen, R. W., "Flowfield in the Combustion Chamber of a Solid Propellant Rocket Motor," *AIAA Journal*, Vol. 12, Oct. 1974, pp. 1440-1442.

[15]Beddini, R. A., "Aerothermochemical Analysis of Erosive Burning in a Laboratory Solid-Rocket Motor," *AIAA Journal*, Vol. 16, Sept. 1978, pp. 898-905.

[16]Olson, R. M. and Eckert, E. R. G., "Experimental Studies of Turbulent Flow in a Porous Circular Tube with Uniform Fluid Injection Through the Tube Wall," *Journal of Applied Mechanics*, Vol. 33, No. 4, 1966, pp. 7-17.

[17]Huesmann, K. and Eckert, E. R. G., "Studies of the Laminar Flow and the Transition to Turbulence in Porous Tubes with Uniform Injection Through the Tube Wall," translated from *Warme-und Stoffubertragung*, Bd. 1, 5.2, 1968, pp. 2-9.

[18]Donaldson, C. duP., "Calculations of Turbulent Shear Flows for Atmospheric and Vortex Motions," *AIAA Journal*, Vol. 10, Jan. 1972, pp. 4-12.

[19]Varma, A. K., Beddini, R. A., Sullivan, R. D., and Donaldson, C. duP., "Application of an Invariant Second-Order-Closure Turbulence Model to the Calculation of Compressible Boundary Layers," AIAA Paper 74-592, June 1974.

[20]Sullivan, R. D., "GYC—A Program to Compute the Turbulent Boundary Layer on a Rotating Cone," Aeronautical Research Associates of Princeton, Princeton, NJ, WP 76-2, 1976.

[21]Pimenta, M. and Moffat, R. J., "Stability of Flow Through Porous Plates: Coalescent Jets Effect," *AIAA Journal*, Vol. 12, Oct. 1974, pp. 1438-1440.

[22]Tong, K. and Knight, C. J., "Flow Around an Isolated Porous Tube with Nonuniform Wall Thickness," *AIAA Journal*, Vol. 17, Nov. 1979, pp. 1262-1263.

[23]Brown, R. S., Willoughby, P. G., and Dunlap, R., "Coupling Between Velocity Oscillations and Solid Propellant Combustion," AIAA Paper 84-0288, Jan. 1984.